

# Magnetization and $^{11}\text{B}$ NMR study of $\text{Mg}_{1-x}\text{Al}_x\text{B}_2$ superconductors

M. Pissas,<sup>1</sup> G. Papavassiliou,<sup>1</sup> M. Karayanni,<sup>1</sup> M. Fardis,<sup>1</sup> I. Maurin,<sup>2</sup> I. Margiolaki,<sup>2</sup> K. Prassides,<sup>1,2</sup> and C. Christides<sup>1,3</sup>

<sup>1</sup>*Institute of Materials Science, NCSR, Demokritos, 153 10 Aghia Paraskevi, Athens, Greece*

<sup>2</sup>*School of Chemistry, Physics and Environmental Science, University of Sussex, Brighton BN1 9QJ, United Kingdom*

<sup>3</sup>*Department of Engineering Sciences, School of Engineering, University of Patras, 26110 Patras, Greece*

(Received 18 January 2002; revised manuscript received 27 February 2002; published 30 April 2002)

We demonstrate the magnetic-field distribution of the pure vortex state in lightly doped  $\text{Mg}_{1-x}\text{Al}_x\text{B}_2$  ( $x \leq 0.025$ ) powder samples, by using  $^{11}\text{B}$  nuclear magnetic resonance in magnetic fields of 23.5 and 47 kOe. The magnetic-field distribution at  $T = 5$  K is Al-doping dependent, revealing a considerable decrease of anisotropy in respect to pure  $\text{MgB}_2$ . This result correlates nicely with magnetization measurements and is consistent with  $\sigma$ -band hole driven superconductivity for  $\text{MgB}_2$ .

DOI: 10.1103/PhysRevB.65.184514

PACS number(s): 74.25.-q, 74.60.-w, 76.60.Es

## I. INTRODUCTION

The synthesis of  $\text{MgB}_2$  had been reported<sup>1</sup> in 1954 but only recently Nagamatsu *et al.*<sup>2</sup> discovered that this compound is a superconductor with a surprisingly high  $T_c \approx 39$  K. At first it was suggested<sup>3</sup> that a BCS-type mechanism with strong electron-phonon coupling and high phonon energy of the light boron atoms can be responsible for the observed high  $T_c$ . This is based on the observation of the isotope effect<sup>4</sup> on  $T_c$  and a strong negative pressure coefficient<sup>5</sup> of  $T_c$ . Alternatively, Hirsch<sup>6</sup> proposed a “universal” mechanism where superconductivity in  $\text{MgB}_2$  is driven by the pairing of dressed holes. Electronic band-structure calculations<sup>3,7–10</sup> indicate that in  $\text{MgB}_2$  the charge carriers are situated in two bands derived from the  $\sigma$  bonding  $p_{x,y}$ -orbitals of boron, which are essentially two dimensional ( $2D$ ), and in one electron and one hole bands derived from the  $\pi$ -bonding  $p_z$  orbitals of boron. Both,  $\sigma$  and  $\pi$  bands have strong in-plane dispersion due to the large overlap between all  $p$  orbitals of neighboring boron atoms. Despite some diversities in these models, there is a general agreement<sup>3,6–8,11,12</sup> that the key point for superconductivity in  $\text{MgB}_2$  is the  $2D$   $\sigma$  band of  $p_{x,y}$  orbitals within the boron layers, and the delocalized metallic-type bonding between these layers. These calculations predict<sup>3,7,13–15</sup> a strong anisotropy in the Fermi surface (and possibly in the electron-phonon coupling) that is consistent with the observed<sup>15–17</sup> anisotropy in  $H_{c2}$ . Specifically, the anisotropic ratio:  $\gamma = H_{c2}^b/H_{c2}^c$ , was found<sup>15,17,18</sup> to be between 1.7 and 6, depending on the material and the experimental method.

In view of this description, measurements on electron- or hole-doped  $\text{MgB}_2$  are of interest as they may help our understanding of how the electronic density of states and the Fermi surface depend on doping. Al substitution for Mg in  $\text{Mg}_{1-x}\text{Al}_x\text{B}_2$  provides<sup>19,20</sup> a way for electron doping. The similarity of the calculated electronic density of states between  $\text{MgB}_2$  and  $\text{AlB}_2$  indicates that doping results in simple filling of the available electronic states, with one electron donated per Al.<sup>8–10</sup> A very first study of Al doped  $\text{MgB}_2$  has shown<sup>19</sup> that  $T_c$  is slightly suppressed for  $x \leq 0.1$ . However, band-structure calculations show<sup>3</sup> that there is a sharp drop

in the density of states of  $\text{MgB}_2$  at only slightly higher electron concentrations. Suzuki *et al.*<sup>10</sup> predict that in  $\text{Mg}_{1-x}\text{Al}_x\text{B}_2$  the concentration of  $\sigma$  holes varies with  $x$  as  $n_h = (0.8 - 1.4x) \times 10^{22} \text{ cm}^{-3}$ , leading to  $n_h = 0$  for  $x \approx 0.6$ . For  $0.1 \leq x \leq 0.25$ , a two phase mixture is formed, whereas for  $x > 0.25$  a single nonsuperconducting phase is detected. The detrimental effect of doping on  $T_c$  in  $\text{Mg}_{1-x}\text{Al}_x\text{B}_2$  can be explained within the BCS model, as it increases the Fermi energy ( $E_F$ ) and decreases the density of states  $N(E_F)$ . Besides, thermoelectric power and resistivity measurements show<sup>21</sup> that  $\text{Mg}_{1-x}\text{Al}_x\text{B}_2$  alloys are hole-type normal metals.

In order to analyze trends associated with the band filling and their relation to loss of superconductivity, we have performed a detailed study of  $\text{Mg}_{1-x}\text{Al}_x\text{B}_2$  ( $0 \leq x \leq 0.1$ ) using structural, magnetic, and  $^{11}\text{B}$  nuclear magnetic resonance (NMR) line-shape measurements. Complementary magnetic and NMR measurements reveal a decrease of anisotropy by slight Al doping relative to pure  $\text{MgB}_2$  samples, providing an experimental evidence about the effect of  $\sigma$ -band hole filling in these superconductors.

## II. EXPERIMENTAL DETAILS

Powder samples with nominal composition  $\text{Mg}_{1-x}\text{Al}_x\text{B}_2$  ( $0 \leq x \leq 1$ ) were prepared by liquid vapor to solid reaction as described elsewhere.<sup>22</sup> Synchrotron x-ray powder-diffraction measurements were performed on  $\text{Mg}_{1-x}\text{Al}_x\text{B}_2$  samples, sealed in thin-wall glass capillaries, 0.5 mm in diameter, at 295 K. Images of the Debye-Scherrer rings were recorded on the 345-mm-diameter Mar Research circular image plate system on the BM1A beam line at the ESRF, Grenoble. A monochromatic x-ray beam of wavelength,  $\lambda = 0.79983$  Å and dimensions  $0.5 \times 0.5 \text{ mm}^2$  was focused onto the sample by sagittal bending of the second crystal of the double-crystal Si(111) monochromator. Patterns were measured with sample-to-detector distance of 200 mm for periods of 10 s. During the data collection the sample was rotated about its axis by  $10^\circ$ . One-dimensional diffraction patterns were obtained by integrating around the rings using local software (program FIT2D). dc-magnetization measurements were performed in a superconducting quantum interference device (SQUID) magnetometer

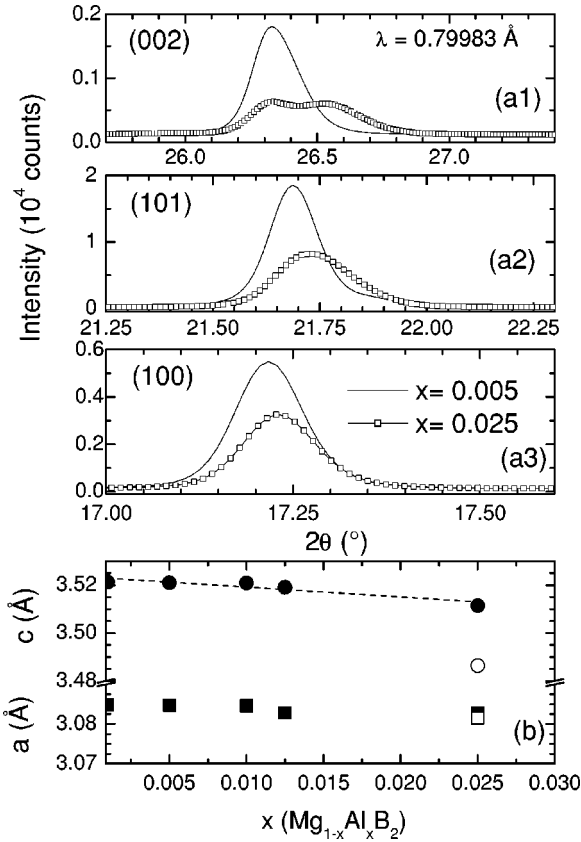


FIG. 1. (a) Synchrotron x-ray diffraction ( $\lambda = 0.79983 \text{ \AA}$ ) profiles showing the (002), (101), and (100) reflections for the  $\text{Mg}_{1-x}\text{Al}_x\text{B}_2$  samples with  $x = 0.005$  and  $0.025$ . (b) Variation of the hexagonal unit-cell parameters of  $\text{Mg}_{1-x}\text{Al}_x\text{B}_2$  for  $0 \leq x \leq 0.025$ . Solid circles and squares correspond to the  $c$  and  $a$  axis of the  $\text{Mg}_{1-x}\text{Al}_x\text{B}_2$  phase, respectively. The corresponding open symbols for  $x = 0.025$  are the cell constants of the second ( $\text{Mg}_{1-x}\text{Al}_x\text{B}_2$ )/phase (see main text).

(Quantum Design) under a magnetic field of  $H = 10 \text{ Oe}$ .  $^{11}\text{B}$  NMR line-shape measurements of the central transition ( $-1/2 \rightarrow 1/2$ ) were performed on two spectrometers operating in external magnetic fields  $H_0 = 23.5$  and  $47 \text{ kOe}$ . The spectra were obtained from the Fourier transform of half of the echo, following a typical  $\pi/2 - \tau - \pi$  spin-echo pulse sequence.<sup>23</sup> The irradiation frequency was the same in all experiments. The spectral bandwidth around the irradiation frequency was  $\approx 150 \text{ kHz}$ , which is enough to cover adequately the NMR signals at low temperatures.

### III. RESULTS AND DISCUSSION

#### A. X-ray measurements

Figure 1(a) shows parts of the x-ray diffraction patterns that reveal a clear splitting of the (002) reflection in  $\text{Mg}_{1.975}\text{Al}_{0.025}\text{B}_2$  whereas the  $\text{Mg}_{1.995}\text{Al}_{0.005}\text{B}_2$  is single phase sample. This implies the onset of macroscopic phase separation with increasing Al content.<sup>20</sup> A similar result has been reported<sup>24</sup> in C-doped  $\text{MgB}_2$ , where the carbon miscibility is also very small as well:  $x < 0.04$ . For this reason we restrict

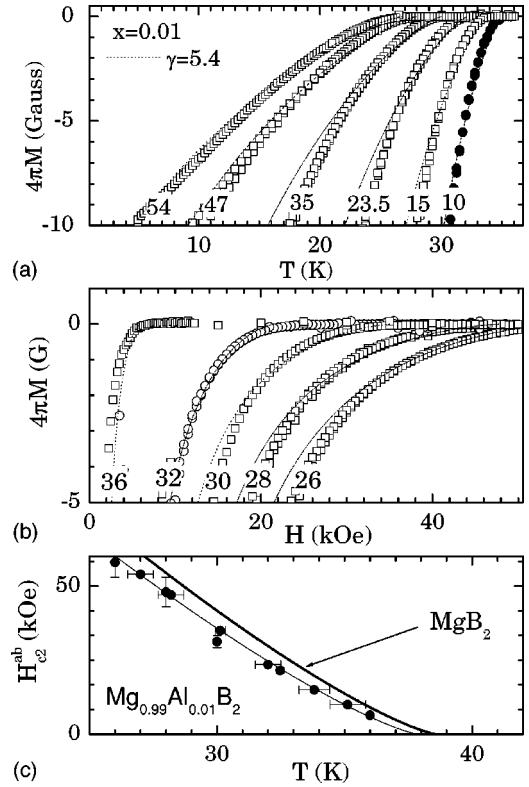


FIG. 2. (a) (upper panel) Zero field and field cooling magnetic moment as a function of the temperature for  $10 \leq H \leq 54 \text{ kOe}$  for the powder  $\text{Mg}_{0.99}\text{Al}_{0.01}\text{B}_2$  sample used in NMR measurements. The dot lines are simulations of the reversible magnetic moment, using a  $\gamma \approx 5.4$  (see main text). (b) (middle panel) Isothermal magnetization loops in the reversible regime at  $26 \leq T \leq 36 \text{ K}$  for  $\text{Mg}_{0.99}\text{Al}_{0.01}\text{B}_2$ . (c) (lower panel) Variation of  $H_{c2}^{ab}$  as a function of temperature for the  $x = 0.01$  sample. The solid line is a fit with a power-law relation  $H_{c2}^{ab} = H^*(1 - T/T_c)^\nu$  ( $H^* = 262 \pm 5 \text{ kOe}$ ,  $T_c = 37.9 \pm 0.1 \text{ K}$ , and  $\nu = 1.27 \pm 0.02$ ). For comparison the  $H_{c2}^{ab}(T)$  curve (thick solid line) of the  $x = 0$  sample is included.

our NMR study only to  $\text{Mg}_{1-x}\text{Al}_x\text{B}_2$  samples with  $x \leq 0.025$ . The deduced lattice parameters are plotted in Fig. 1(b). For  $x < 0.025$ , the  $c$  axis exhibits a negative slope:  $dc/dx \approx (-0.2 \text{ \AA/at. \% Al})$ , whereas the in-plane  $a$  axis remains nearly constant. For  $x \geq 0.025$ , the coexisting phases differ mainly in their interlayer lattice constant.

#### B. Magnetic measurements

Thermomagnetic measurements show that all the examined samples are superconductors, with their  $T_c$  decreasing quasilinearly with increasing Al content ( $dT_c/dx \approx -0.1 \text{ K/at. \% Al}$ ). A steeper decrease of  $T_c$  is observed for  $x > 0.1$  and  $T_c$  becomes zero at  $x \approx 0.55$ . Figure 2 shows the reversible portion of the temperature dependence of the magnetization in various fields for  $x = 0.01$ . Contrary to the expected linear behavior, the  $M(T)$  curves exhibit a pronounced curvature nearby the  $T_{c2}(H)$  that is attributed<sup>17,18</sup> to the anisotropy of  $\text{MgB}_2$ . The dot lines through the experimental points come from a simulation of the reversible magnetic moment using the equation<sup>17</sup>

$$4\pi M = - \frac{\Phi_0}{8\pi\lambda(T)^2\beta_A\gamma^{1/3}\sqrt{\gamma^2-1}} \left[ \frac{1-4h^2}{3h^2}\sqrt{1-h^2} + \ln\left(\frac{1+\sqrt{1-h^2}}{h}\right) \right], \quad (1)$$

where  $h = H/H_{c2}^{ab}$ ,  $\lambda = (\lambda_{ab}^2\lambda_c)^{1/3}$  is the average penetration depth,  $\beta_A = 1.16$ ,  $\Phi_0$  is the flux quantum, and  $\gamma = H_{c2}^{ab}/H_{c2}^c$  is the anisotropy constant. To simulate the  $M(T)$  data we assume first, a power-law relation:  $H_{c2}^{ab}(T) = H^*(1 - T/T_c)^\nu$  ( $H^* = 262 \pm 25$  kOe,  $T_c = 37.9 \pm 0.1$  K, and a  $\nu = 1.27 \pm 0.05$ ), second, a  $\lambda \sim 200$  nm, and third, an anisotropy constant  $\gamma \sim 5.4$ .

It is important to note that the power-law variation of  $H_{c2}^{ab}$  concerns only the region  $T > T_c/2$ . At lower temperatures the  $H_{c2}^{ab}$  exhibits a negative curvature<sup>18</sup> and approaches saturation at  $T = 0$  K at a value of about 140 kOe. Assuming that:  $H_{c2}^{ab}$  is about 140 kOe in both samples ( $x = 0$  and 0.01), with a  $\gamma = 6$  or 5.6, then the estimated  $H_{c2}^c$  will be 23.3 kOe and 25 kOe, respectively. Also, we find that the temperature dependence of  $H_{c2}^{ab}$  has the same functional form for  $x = 0.01$  and  $x = 0$  (i.e., the same exponent) whereas for  $x = 0.01$  the  $T_c$  and the  $H^*$  values are smaller by 0.7 K and 20 kOe respectively. Similarly, the  $M(H)$  data have been simulated by using the same  $\gamma$  and a temperature depended  $\lambda(T)$ . In agreement with the NMR spectra (vide infra) for  $x = 0.01$ , the deduced value of the anisotropy constant from magnetic measurements is *smaller than* the anisotropy constant of pure  $\text{MgB}_2$  ( $\gamma \sim 6$ ). It is worth noting here that both, the pure and Al-doped samples were prepared with the same method. Thus, the obtained differences in  $\gamma$  cannot be attributed in the preparation method used. To cross-check the validity of the estimated  $\gamma$  values we have applied an alternative simulation method,<sup>18</sup> that was used by Bud'ko *et al.* in pure  $\text{MgB}_2$  powder samples, and we have obtained exactly the same values.

### C. $^{11}\text{B}$ NMR measurements

Generally, vortices at low temperature form a lattice in the mixed state of type-II superconductors,<sup>25</sup> generating a spatial field modulation that gives rise to a characteristic magnetic-field distribution  $f(H)$  with van Hove singularities. For a perfect vortex lattice the field distribution exhibits a peak at a value  $H_s$ , which corresponds to the saddle point located midway between two vortices, whereas two steps at the maximum ( $H_{\max}$ ) and minimum ( $H_{\min}$ ) fields are expected.<sup>26,27</sup> Other studies have<sup>27,28</sup> shown that the  $f(H)$  is reflected on NMR line shapes because the Larmor frequency of the resonating nuclei depends linearly on the local magnetic field. Thus, NMR is a very sensitive local probe of the spatially inhomogeneous magnetic field associated with the vortex state,<sup>26,27</sup> which is formed in external magnetic fields  $H_{c1} < H_0 < H_{c2}$ . In case of strong anisotropy and in applied field  $H_{c2}^c < H_0 < H_{c2}^{ab}$ , a powder superconducting sample with randomly oriented grains is expected to give a superposition

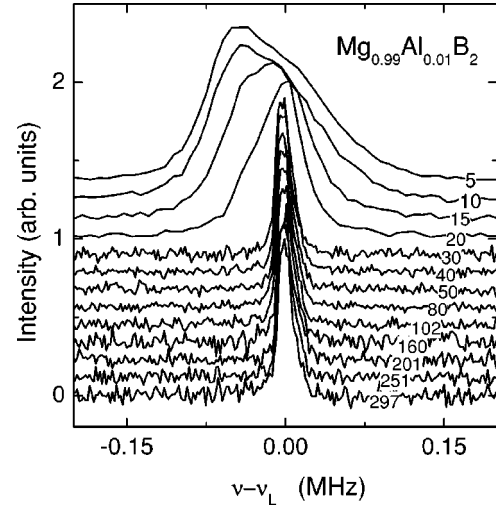


FIG. 3.  $^{11}\text{B}$  NMR line shapes as a function of temperature for  $\text{Mg}_{0.99}\text{Al}_{0.01}\text{B}_2$  under a magnetic field  $H = 23.5$  kOe. Each spectrum is normalized to its maximum intensity for clarity.

of magnetic-field distributions, ranging in between the normal state and the Abrikosov lattice. In a recent study<sup>23</sup> it was observed that the  $^{11}\text{B}$  NMR line shapes in pure  $\text{MgB}_2$  remain unchanged down to the temperature of the second critical field  $T_{c2}$  whereas for  $T < T_{c2}$ , a second peak develops at lower frequencies. The intensity ratio of this second peak to the unshifted high- $T$  peak was observed to increase in field  $H_0 = 23.5$  kOe when compared<sup>23</sup> with that in field  $H_0 = 47$  kOe. A direct comparison of the NMR line shapes with dc-magnetic measurements, that reveal the temperature dependence of  $H_{c2}^{ab}$  and  $H_{c2}^c$ , has shown that the frequency position and the shape of the low-frequency peak follows the development of the vortex lattice as a function of temperature.<sup>23</sup> Since in pure  $\text{MgB}_2$ ,  $H_{c2}^{ab} \approx 140$  kOe,<sup>15,17</sup> this was explained by considering that a part of the grains remains in the normal state (unshifted peak) down to the lowest measured temperature  $T = 5$  K when  $H_{c2}^c < H_0 < H_{c2}^{ab}$ .

Figure 3 shows the  $^{11}\text{B}$  NMR line shapes for  $x = 0.01$  in 23.5 kOe as a function of temperature. As in  $\text{MgB}_2$  spectra,<sup>23</sup> the line shapes in the normal state are temperature independent. For  $T \leq 30$  K the vortex lattice is formed, inducing a gradual shift of the peak frequency (corresponding to  $H_s$ ) that creates the characteristic asymmetric broadening of the NMR frequency distribution as expected from the vortex lattice only.<sup>26</sup> Remarkably, the normal-state signal component disappears in the mixed superconducting state by light Al doping, and only the pure vortex lattice signal is present. This effect indicates an enhancement (relative to pure  $\text{MgB}_2$ ) of  $H_{c2}^c$  above 23.5 kOe by Al doping, which gives rise to the pure superconducting state at low temperatures. At  $T = 5$  K the shift of  $H_s$  from the field  $H_0$  in the normal state is about 50 Oe. However, the expected<sup>29</sup> sharp singularities in the field distribution function  $f(H)$  of the vortex lattice are smeared out in our NMR spectra because we measure an anisotropic polycrystalline sample. Thus, we cannot

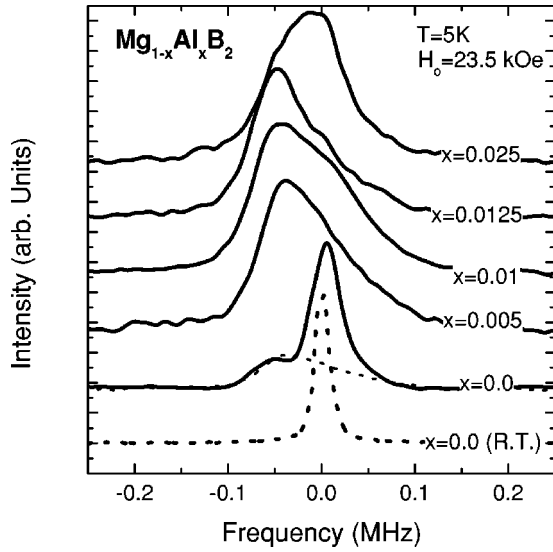


FIG. 4.  $^{11}\text{B}$  NMR line shapes of  $\text{Mg}_{1-x}\text{Al}_x\text{B}_2$  for  $0.0 \leq x \leq 0.025$  at  $T=5$  K in a field  $H_0=23.5$  kOe. Each spectrum is normalized to its maximum intensity for clarity.

estimate<sup>28</sup> whether a square or triangular type of vortex lattice is formed.

Figure 4 shows NMR spectra at  $T=5$  K in  $H_0=23.5$  kOe for  $\text{Mg}_{1-x}\text{Al}_x\text{B}_2$  ( $0 \leq x \leq 0.025$ ). At  $T=300$  K the NMR spectra are essentially identical for  $0 \leq x \leq 0.2$ . Since the cell constants change slightly in this concentration region, the observed similarity in the NMR spectra indicates that the induced line shape is resolution limited. At  $T=5$  K all the samples are in the mixed state and the line shape reflects the magnetic-field distribution from the vortex lattice. Remarkably, the line shapes depend on  $x$ . As discussed above for the  $x=0$  system, the observed line shape is the result of the anisotropy. Hence, the disappearance of the normal-state signal component and the variation of the vortex state signal with  $x$  can be explained by assuming that the anisotropy decreases with Al doping. For comparison we have scaled the signal intensity of the  $x=0.005$  system under the low-frequency tail of pure  $\text{MgB}_2$  in Fig. 4. Apparently there is an excellent matching of the two signals, providing clear experimental evidence that this shoulder corresponds to the magnetic-field distribution of the vortex state. Thus, it becomes evident that even for  $x=0.005$  the component from the normal-state signal disappears. We also notice that for  $x \geq 0.025$  the line shape changes drastically. This can be explained by considering that either the anisotropy starts to increase abruptly or the particular line shape is associated with the onset of phase separation at this composition. Figure 5 shows the dependence of the NMR spectra on Al doping for  $\text{Mg}_{1-x}\text{Al}_x\text{B}_2$  ( $0 \leq x \leq 0.025$ ), at  $T=5$  K and  $H_0=47$  kOe. Contrary to Fig. 4, in all samples the line shapes exhibit a low-frequency tail and an unshifted peak, corresponding to coexisting vortex and normal-state components. This indicates that  $3.2 \leq \gamma \leq 6.4$  (e.g., for  $x=0.01$  sample) by considering  $H_{c2}^{ab} \approx 140$  kOe.

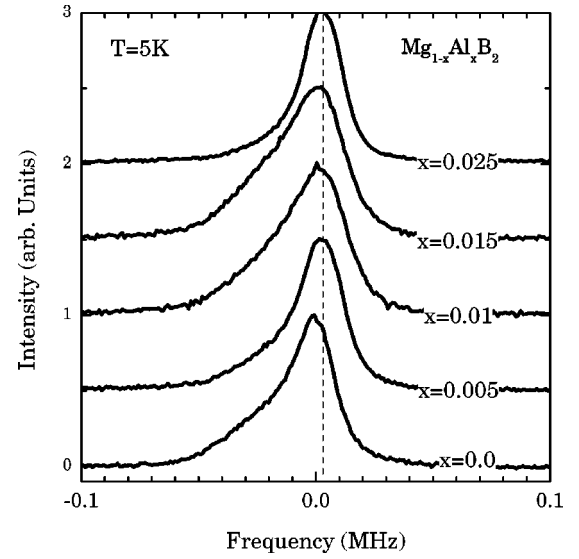


FIG. 5.  $^{11}\text{B}$  NMR line shapes of  $\text{Mg}_{1-x}\text{Al}_x\text{B}_2$  for  $0.0 \leq x \leq 0.025$  at  $T=5$  K in a magnetic field  $H_0=47$  kOe. Each spectrum is normalized to its maximum intensity for clarity.

Results of Knight shift and nuclear spin-lattice relaxation rates ( $1/T_1$ ) for  $^{25}\text{Mg}$ ,  $^{11}\text{B}$ , and  $^{27}\text{Al}$  nuclei were reported for  $\text{MgB}_2$ ,  $\text{AlB}_2$ , and  $(\text{Mg}_{1-x}\text{Al}_x)\text{B}_2$  powder samples.<sup>30–33</sup> The comparison of the data in the two compounds shows the dramatic drop of the density of states at the boron site<sup>32,33</sup> in  $\text{AlB}_2$  and  $(\text{Mg}_{1-x}\text{Al}_x)\text{B}_2$  with respect to  $\text{MgB}_2$ . In addition, the discrepancies in the results of  $1/T_1$  below  $T_c$ , reported by different authors, can be explained<sup>32</sup> by the strong anisotropy of the upper critical field in  $\text{MgB}_2$ . In this study the observed decrease of anisotropy, by substituting Al for Mg, can be attributed to the progressive electron filling of the  $\sigma$  bands with increasing  $x$ , which reduces the anisotropy of the boron  $p$  states. It is worth noting that we could not estimate the absolute anisotropy constant, but we have found that the anisotropy in Al-doped samples is smaller than the value of the  $x=0$  sample. In the microscopic theory the anisotropy parameter is given<sup>34</sup> by  $\gamma^2 = \langle \Delta(\mathbf{k}_F) v_{ab}^2 \rangle / \langle \Delta(\mathbf{k}_F) v_c^2 \rangle$ , where  $v_i$  are the Fermi velocities and  $\langle \dots \rangle$  stands for Fermi-surface averages. When the ratio  $\langle v_{ab}^2 \rangle / \langle v_c^2 \rangle$  is averaged over the entire Fermi surface for  $\text{MgB}_2$  it is close to unity,<sup>3,18</sup> which means a strong anisotropy of  $\Delta(\mathbf{k}_F)$ . Following the arguments of Bud'ko *et al.*,<sup>18</sup> the electron-phonon interaction is particularly strong on the Fermi-surface sheets that are shaped as slightly distorted cylinders along the  $c$ -axis crystal direction. If the gap  $\Delta$  on the remaining Fermi-surface sheets is negligible, the reduction of the anisotropy could originate from the reduction of the  $\sigma$  holes, as mentioned above.

#### IV. CONCLUSION

In conclusion, we show the magnetic-field distribution in the pure vortex state of lightly doped  $\text{Mg}_{1-x}\text{Al}_x\text{B}_2$  by using  $^{11}\text{B}$  NMR line-shape measurements. Our NMR and magnetization data reveal that substitution of Al for Mg reduces the anisotropy substantially. According to current theoretical



models this behavior can be explained only if we consider a reduction of the  $\sigma$  holes. We argue that our results provide an experimental basis for further theoretical investigations concerning the important role of  $p_{x,y}$  orbitals (which form the  $2D$   $\sigma$ -holes band) in the superconductivity of  $\text{MgB}_2$ .

## ACKNOWLEDGMENTS

We thank the ESRF for provision of synchrotron x-ray beamtime and P. Pattison and I. A. Beukes for help with the experiments.

- <sup>1</sup>M. Jones and R. March, J. Am. Chem. Soc. **76**, 1434 (1954).
- <sup>2</sup>J. Nagamatsu, N. Nakagawa, Y. Z. Murakana, and J. Akimitsu, Nature (London) **410**, 63 (2001); C. Buzea and T. Yamashita, Supercond. Sci. Technol. **14**, R115 (2001) (for a recent review).
- <sup>3</sup>J. Kortus, I. I. Mazin, K. D. Belashchenko, V. P. Antropov, and L. L. Boyer, Phys. Rev. Lett. **86**, 4656 (2001).
- <sup>4</sup>S. L. Bud'ko, G. Lapertot, C. Petrovic, C. E. Cunningham, N. Anderson, and P. C. Canfield, Phys. Rev. Lett. **86**, 1877 (2001); D. G. Hinks, H. Claus, and J. D. Jorgensen, Nature (London) **411**, 457 (2001).
- <sup>5</sup>K. Prassides, Y. Iwasa, T. Ito, Dam. H. Chi, K. Uehara, E. Nishibori, M. Takata, M. Sakata, Y. Ohishi, O. Shimomura, T. Muranaka, and J. Akimitsu, Phys. Rev. B **64**, 012509 (2001); B. Lorenz, R. L. Meng, and C. W. Chu, *ibid.* **64**, 012507 (2001).
- <sup>6</sup>J. E. Hirsch and F. Marsiglio, Phys. Rev. B **64**, 144523 (2001).
- <sup>7</sup>J. M. An and W. E. Pickett, Phys. Rev. Lett. **86**, 4366 (2001).
- <sup>8</sup>K. D. Belashchenko, M. van Schilfhaarde, and V. P. Antropov, Phys. Rev. B **64**, 092503 (2001); K. D. Belashchenko, V. P. Antropov, and S. N. Rashkeev, *ibid.* **64**, 132506 (2001).
- <sup>9</sup>G. Satta, G. Profeta, F. Bernardini, A. Continenza, and S. Massidda, Phys. Rev. B **64**, 104507 (2001).
- <sup>10</sup>S. Suzuki, S. Higai, and K. Nakao, J. Phys. Soc. Jpn. **70**, 1206 (2001).
- <sup>11</sup>Y. Kong, O. V. Dolgov, O. Jepsen, and O. K. Andersen, Phys. Rev. B **64**, 020501(R) (2001).
- <sup>12</sup>P. P. Singh, Phys. Rev. Lett. **87**, 087004 (2001).
- <sup>13</sup>Y. Wang, T. Plackowski, and A. Junod, Physica C **355**, 179 (2001).
- <sup>14</sup>F. Bouquet, R. A. Fisher, N. E. Phillips, D. G. Hinks, and J. D. Jorgensen, Phys. Rev. Lett. **87**, 047001 (2001).
- <sup>15</sup>O. F. de Lima, R. A. Ribeiro, M. A. Avila, C. A. Cardoso, and A. A. Coelho, Phys. Rev. Lett. **86**, 5974 (2001); S. Lee, H. Mori, T. Masui, Y. Eltsev, A. Yamamoto, and S. Tajima, J. Phys. Soc. Jpn. **70**, 2255 (2001); M. Xu, H. Kitazawa, Y. Takano, J. Ye, K. Nishida, H. Abe, A. Matsushita, N. Tsujii, and G. Kido, Appl. Phys. Lett. **79**, 2779 (2001).
- <sup>16</sup>S. Patnaik, L. D. Cooley, A. Gurevich, A. A. Polyanskii, J. Jiang, X. Y. Cai, A. A. Squitieri, M. T. Naus, M. K. Lee, J. H. Choi, L. Belenky, S. D. Bu, J. Letteri, X. Song, D. G. Schlom, S. E. Babcock, C. B. Eom, E. E. Hellstrom, and D. C. Larbalestier, Supercond. Sci. Technol. **14**, 315 (2001).
- <sup>17</sup>F. Simon, A. Janossy, T. Feher, F. Muranyi, S. Garaj, L. Forro, C. Petrovic, S. L. Bud'ko, G. Lapertot, V. G. Kogan, and P. C. Canfield, Phys. Rev. Lett. **87**, 047002 (2001).
- <sup>18</sup>S. L. Bud'ko, V. G. Kogan, and P. C. Canfield, Phys. Rev. B **64**, 180506 (2001); S. L. Bud'ko, *et al.*, cond-mat/0201085, Phys. Rev. B (to be published).
- <sup>19</sup>J. S. Slusky, N. Rogado, K. A. Regan, M. A. Hayward, P. Khalifah, T. He, K. Inumaru, S. M. Loureiro, M. K. Haas, H. W. Zandbergen, and R. J. Cava, Nature (London) **410**, 343 (2001).
- <sup>20</sup>J. Y. Xiang, D. N. Zheng, J. Q. Li, L. Li, P. L. Lang, H. Chen, C. Dong, G. C. Che, Z. A. Ren, H. H. Qi, H. Y. Tian, Y. M. Ni, and Z. X. Zhao, cond-mat/0104366 (unpublished); J. Q. Li, L. Li, F. M. Liu, C. Dong, J. Y. Xiang, and Z. X. Zhao, Phys. Rev. B **65**, 132505 (2002); H. W. Zandbergen, M. T. Wu, H. Jiang, M. A. Hayward, M. K. Haas, and R. J. Cava, Physica C **366**, 221 (2002).
- <sup>21</sup>B. Lorenz, R. L. Meng, Y. Y. Xue, and C. W. Chu, Phys. Rev. B **64**, 052513 (2001).
- <sup>22</sup>M. Pissas, E. Moraitakis, D. Stamopoulos, G. Papavassiliou, V. Psycharis, and S. Koutandos, J. Supercond. **14**, 615 (2001).
- <sup>23</sup>G. Papavassiliou, M. Pissas, M. Fardis, M. Karayanni, and C. Christides, Phys. Rev. B **65**, 012510 (2002).
- <sup>24</sup>T. Takenobu, T. Ito, D. H. Chi, K. Prassides, and Y. Iwasa, Phys. Rev. B **64**, 134513 (2001); I. Maurin *et al.*, Physica B (to be published).
- <sup>25</sup>E. H. Brandt, Physica C **369**, 10 (2002).
- <sup>26</sup>E. H. Brandt and A. Seeger, Adv. Phys. **35**, 189 (1986).
- <sup>27</sup>W. Fite and A. G. Redfield, Phys. Rev. Lett. **17**, 381 (1966).
- <sup>28</sup>K. H. Lee, B. J. Mean, G. S. Go, S. W. Seo, K. S. Han, D. H. Kim, H. Lee, B. K. Cho, and S. I. Lee, Phys. Rev. B **62**, 123 (2000).
- <sup>29</sup>A. Rigamonti, F. Borsa, and P. Carretta, Rep. Prog. Phys. **61**, 1367 (1998), see Fig. 4.
- <sup>30</sup>M. Mali, J. Roos, A. Shengelaya, H. Keller, and K. Conder, Phys. Rev. B **65**, 100518 (2002).
- <sup>31</sup>J. K. Jung, S. H. Baek, F. Borsa, S. L. Bud'ko, G. Lapertot, and P. C. Canfield, Phys. Rev. B **64**, 012514 (2001).
- <sup>32</sup>S. H. Baek, B. J. Suh, E. Pavarini, F. Borsa, R. G. Barnes, S. L. Bud'ko, and P. C. Canfield, cond-mat/0201450 (unpublished).
- <sup>33</sup>H. Kotegawa, K. Ishida, Y. Kitaoka, T. Muranaka, N. Nakagawa, H. Takagiwa, and J. Akimitsu, cond-mat/0201578 (unpublished).
- <sup>34</sup>L. P. Gor'kov and T. K. Melik-Barkhudarov, Zh. Éksp. Teor. Fiz. **45**, 1493 (1963) [Sov. Phys. JETP **18**, 1031 (1964)].